

Development, characterization, sintering, dielectric and optical properties of $\text{NdBa}_2\text{ZrO}_{5.5}$ nanocrystals

V RATHEESH KUMAR, P R S WARIAR*, R PAZHANI†, J K THOMAS†, R JOSE§ and J KOSHY

Department of Physics, University College, Trivandrum 695 034, India

†Department of Physics, Mar Ivanios College, Trivandrum 695 015, India

§University of Malaysia Pahang, 26300 Kuantan, Malaysia

MS received 3 September 2010; revised 5 August 2011

Abstract. Nanocrystalline $\text{NdBa}_2\text{ZrO}_{5.5}$ has been successfully synthesized through a single step auto-ignition combustion route for the first time. X-ray diffraction and Fourier transform infrared spectroscopy revealed that the combustion product is phase pure and has an ordered cubic perovskite structure. The phase transitions and thermal stability of the nanopowder were investigated by differential thermal and thermogravimetric analyses. Transmission electron microscopy results indicated that the particle sizes are 20–30 nm. Selected area electron diffraction pattern has shown that as-prepared powder is polycrystalline in nature. The optical absorption spectra analysis confirmed that the material falls to the semiconducting range with a bandgap of ~ 3.69 eV and therefore, could be used as transparent wide bandgap semiconductor. The relative density of the sintered sample is $\sim 96\%$ at 1510°C for 2 h. The surface morphology of the sintered pellet has been studied by scanning electron microscopy and the average grain size observed is ~ 0.7 μm . Dielectric constant (ϵ_r) of $\text{NdBa}_2\text{ZrO}_{5.5}$ at 5 MHz is 29.6 and loss factor ($\tan \delta$) is 4×10^{-2} at room temperature.

Keywords. Perovskites; nanoparticles; combustion synthesis; dielectric properties; energy bandgap.

1. Introduction

Materials with perovskite-type structure are attracting intense interest in many applied and fundamental areas of solid-state science and advanced materials research. This is because of a broad range of physical and chemical properties (Kimura and Tokura 2000; Lichtenburg *et al* 2001) of these types of materials. Perovskites have a general stoichiometry, ABO_3 and are formed by a network of corner sharing BO_6 octahedra, in which all oxygen atoms are in two-coordinate, bridging positions between adjacent B sites; the dodecahedral interstices of the oxygen sub-lattice is occupied by a second cation A . Perovskites exist in different crystal structures due to the feasibility of substituting, either partially or fully, alkaline earth, rare earth and transition metal ions in the A and B sites of perovskite unit cell. The substitution results in an arrangement of the cations either orderly or randomly in A and B sites of the basic perovskite unit cell, thereby, forming a complex perovskite structure. Transition metals, which usually occupy the B -sublattice of the perovskite-type structure, have their frontier d -orbitals close in energy to the $\text{O}(2p)$ orbitals. The electronic structure of the perovskite-type oxides near the Fermi level is, therefore, dominated by the hybridization of these orbitals (Goodenough 1971). The top of the valence band is predominantly formed by the $\text{O}(2p)$ orbitals, whereas bottom

of the conduction band consists mainly of d -orbitals of the transition metal. The bandgap energy is one of the important properties of functional materials for photochemical applications (Osterloh 2008). In d^0 perovskite-type oxides, the bandgap energy is determined by the difference between energy of the d -orbitals of the transition metals and $\text{O}(2p)$ orbitals.

In view of their chemical stability, synthesis of $\text{NdBa}_2\text{ZrO}_{5.5}$, a complex perovskite oxide, has been investigated for possible applications as substrates for high T_C superconductors (HTS) and in these investigations, $\text{NdBa}_2\text{ZrO}_{5.5}$ was synthesized through solid state route (Tovar *et al* 2007). However, a single phase $\text{NdBa}_2\text{ZrO}_{5.5}$ could be obtained through solid state reaction route only after prolonged calcinations of the reaction mixture at 1000°C for 38 h with multiple intermediate grindings. Also we have not reported the sintering behaviour or dielectric properties of $\text{NdBa}_2\text{ZrO}_{5.5}$.

Synthesis of advanced ceramics as nanocrystals is one of the major fields in materials processing technology (Glieter 2000; Karagedov and Lyakhov 1999; Ravichandran *et al* 2004) and the advantages of nanocrystalline materials over microstructured materials are superior phase homogeneity, sinterability and microstructure leading to unique mechanical, electrical, dielectric, magnetic, optical and catalytic properties (Suryanarayana 1994; Skandan *et al* 1999). The coarse-grained powders synthesized using the conventional solid state route have disadvantages like larger particle size, high temperature processing and relatively lower phase

*Author for correspondence (prswariar@yahoo.com)

purity. In this paper, we report the synthesis, characterization, sintering behaviour, optical and dielectric properties of single phase nanoparticles of $\text{NdBa}_2\text{ZrO}_{5.5}$, for the first time. The product was characterized by XRD, TGA/DTA, FT-IR, UV-VIS, TEM and SEM.

2. Experimental

The basic step for the synthesis of $\text{NdBa}_2\text{ZrO}_{5.5}$ nanoparticles was to prepare an aqueous solution containing Ba^{2+} , Nd^{3+} and Zr^{4+} ions by dissolving stoichiometric amounts of high purity $\text{Ba}(\text{NO}_3)_2$ (99.9%, CDH), Nd_2O_3 (99.9%, CDH) and $\text{ZrOCl}_2 \cdot 8\text{H}_2\text{O}$ (99.5%, Sigma-Aldrich) in suitable solvents. Nd_2O_3 was dissolved in 0.1N nitric acid, $\text{Ba}(\text{NO}_3)_2$ and $\text{ZrOCl}_2 \cdot 8\text{H}_2\text{O}$ in double distilled water. The solutions were mixed together in a glass beaker and sufficient amount of citric acid (99%, CDH) was added to the solution containing metal ions to get the precursor complex, maintaining the citric acid to cation ratio at unity. Subsequently, nitric acid and ammonium hydroxide were added to the system to adjust the oxidant/fuel ratio, where nitric acid acted as the oxidant and liquor ammonia acted as the fuel. The solution containing the complex precursor at neutral pH was then heated to about 250 °C on a hot plate. The solution boiled on heating and formed a syrupy liquid, which underwent dehydration and decomposition leading to smooth deflation producing foam. The foam then ignited by itself on persistent heating giving voluminous and fluffy product of combustion. The combustion product was subsequently characterized as single phase nanocrystals of $\text{NdBa}_2\text{ZrO}_{5.5}$.

The as-synthesized $\text{NdBa}_2\text{ZrO}_{5.5}$ nanoparticles were characterized for crystal phase identification by powder X-ray diffraction (XRD) technique using a X-ray Diffractometer (Model Bruker D-8) with nickel filtered $\text{CuK}\alpha$ radiations ($\lambda = 0.15406$ nm) in the range of 2θ between 20° and 70°. The infrared spectra (IR) of the samples were recorded in the range 400–4000 cm^{-1} on a Thermo-Nicolet Avatar 370 Fourier Transform Infrared (FT-IR) Spectrometer. Samples were prepared by mixing dried $\text{NdBa}_2\text{ZrO}_{5.5}$ nanoparticles with KBr and pressing them into pellets. The thermal decomposition behaviour of the powder was studied by differential thermal analysis (DTA) and thermogravimetric analysis (TGA) using a simultaneous Perkin-Elmer TG/DTA thermal analyser in the range 40–1100 °C at a heating rate of 20 °C/min in nitrogen atmosphere. The optical absorption spectrum of the nanopowder at room temperature was obtained using a Cary 100 BIO UV-VIS Spectrophotometer in the wavelength range 190–900 nm. The morphology of the nanocrystallites was inspected using a transmission electron microscope (TEM, JEOL 2010Fas) with an accelerating voltage of 200 kV. For TEM observation, the powder samples were dispersed in methanol and sonicated for 30 min to obtain better particle dispersion and allowing a drop of this to dry on a carbon-coated copper grid.

To study sinterability of the $\text{NdBa}_2\text{ZrO}_{5.5}$ nanoparticles obtained by the present combustion method, the combustion

derived powders were mixed with 5% polyvinyl alcohol as binder and uniaxially pressed in the form of circular discs of 14 mm diameter and ~2 mm thickness at a pressure of about 350 MPa using a hydraulic press. The binder was removed by heating the pellet at 600 °C for 30 min. The pellet was then sintered at 1510 °C for 2 h in a programmable furnace in air at a heating/cooling rate of 10 °C/min. The density of the sintered specimen was measured using Archimedes method with distilled water as the liquid medium. The microstructure of sintered samples after thermal etching was investigated by scanning electron microscope (JEOL, Model-JSM-6390LA, Analytical SEM).

The simplest way to measure the dielectric constant of a material is based on the measurement of capacitance of capacitor using the material, whose dielectric constant is to be measured, as the dielectric medium between a parallel plate or co-axial capacitor. The capacitance (C) of a capacitor is related to dielectric constant ϵ_r as

$$C = \frac{\epsilon_0 \epsilon_r A}{d}, \quad (1)$$

where A is the cross-sectional area of the capacitor, d the thickness of the dielectric material and ϵ_0 the permittivity of free space (8.85×10^{-12} F/m). The capacitance and loss tangent measurements were carried out on the sample in the form of pellet of about 10.48 mm in diameter and 1.68 mm in thickness using an LCR meter (HIOKI 3532–50). For dielectric measurements, silver electrodes were attached on either sides of the sintered pellet and dried at 80 °C for 15 min. The dielectric constant and loss factor were calculated as a function of frequency (1 kHz–5 MHz).

3. Results and discussion

3.1 XRD analysis

Figure 1 shows XRD pattern of as-prepared $\text{NdBa}_2\text{ZrO}_{5.5}$ powder obtained by the present combustion synthesis. All the peaks are indexed for a complex cubic ($Fm\bar{3}m$) perovskite structure and the lattice constant calculated from the XRD data is $a = 8.408$ Å and it agrees very well with the reported XRD data in the JCPDS cards No. 47–0387. The crystallite size calculated from full width at half-maximum (FWHM) using Scherrer formula is

$$D = \frac{k\lambda}{\beta \cos \theta}, \quad (2)$$

where λ is the wavelength of the X-ray, β the full width at half maximum (FWHM) of a diffraction peak, θ the diffraction angle and k the Scherrer's constant of the order of unity for usual crystal (~0.9). The average particle size obtained from the XRD data for (220) plane in figure 1 is ~24 nm. No diffraction peak that could be related to impurity or secondary phase was observed in the XRD pattern. This shows that by adopting combustion method, phase pure and well crystalline powders of perovskite materials can be prepared

within a short duration without the need for a calcinations step. It may be noted that a single phase $\text{NdBa}_2\text{ZrO}_{5.5}$ can be obtained through a solid state reaction route only after prolonged calcinations of the reaction mixture at 1000°C with multiple intermediate grindings. Thus combustion process has energy and cost saving advantages.

3.2 FT-IR spectrum analysis

Figure 2 shows FT-IR spectrum of a typical as-prepared $\text{NdBa}_2\text{ZrO}_{5.5}$ powder. The asymmetric stretching and bending modes of the BO_6 octahedra, usually dominate the IR spectra of perovskite materials (Ratheesh *et al* 1997). Therefore, in the present case, the strong band from 400 cm^{-1} is involving the asymmetric bending mode, $\nu_4(T_{1u})$ of the ZrO_6

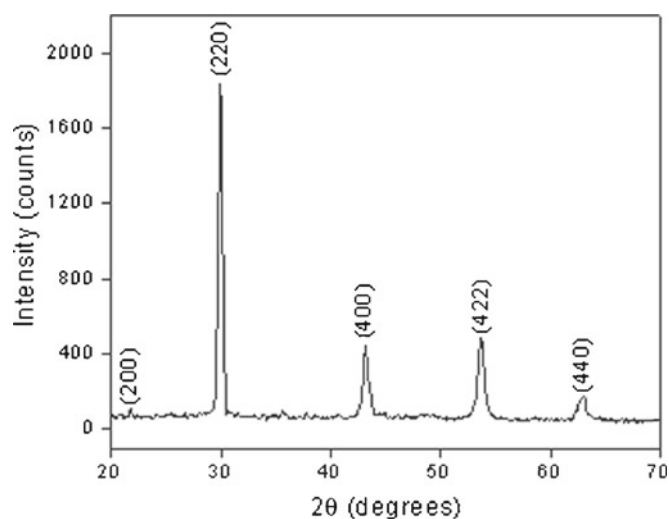


Figure 1. Powder XRD pattern of as-prepared $\text{NdBa}_2\text{ZrO}_{5.5}$ nanopowder.

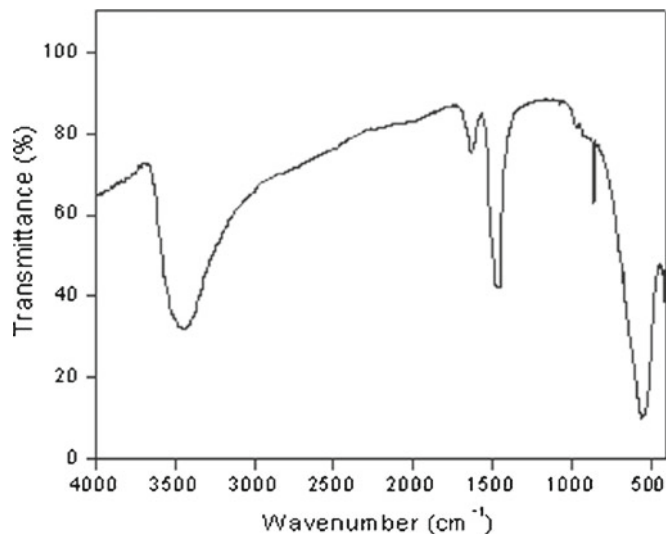


Figure 2. FT-IR spectrum of as-prepared $\text{NdBa}_2\text{ZrO}_{5.5}$ nanopowder.

octahedra whilst the other strong broad band from 550 cm^{-1} can be assigned to the asymmetric stretching mode, $\nu_3(T_{1u})$ of the ZrO_6 octahedra. The same spectral pattern, with two strong and well defined IR bands in the $400\text{--}600\text{ cm}^{-1}$ region, has also been found in a great number of $\text{A}_2\text{BB}'\text{O}_6$ perovskite type materials and they were assigned in the same way (Corsmit *et al* 1972; Blasse and Corsmit 1973; Zheng *et al* 1998; Lavat *et al* 2001). Finally, the weak band from 864 cm^{-1} can be assigned to the originally IR inactive symmetric stretching mode, $\nu_1(A_{1g})$ of the ZrO_6 octahedra, activated by symmetry lowering. The absorption bands around $1500\text{--}1700\text{ cm}^{-1}$ and $1300\text{--}1500\text{ cm}^{-1}$ are assigned to water bending vibration, and CO_2 characteristic vibrations, respectively (Nyquist and Kagel 1971; Nakamoto 1986). The broad feature in the $3000\text{--}3600\text{ cm}^{-1}$ region is attributed to O-H stretching of physisorbed water or from surface-adsorbed hydroxyl groups. Thus, there was no evidence for the presence of any organic matter in the sample.

3.3 Thermal analysis

Figure 3 shows typical DTA and TGA curves of the as-prepared powders of $\text{NdBa}_2\text{ZrO}_{5.5}$ up to 1100°C . TGA curve shows a weight loss of $\sim 4\%$ at about 100°C , which can be caused by the adsorbed moisture in the sample. The weight change corresponds to an endotherm on the DTA curve around 100°C . Thereafter, there is no substantial weight change or enthalpy change occurring in the sample at temperatures up to 1100°C , which implies that the combustion is complete and no organic matter is present in the sample. There is also no evidence of any phase transition taking place in the sample up to this temperature.

3.4 TEM analysis

TEM studies on the powder morphology of the as-prepared powder obtained by the combustion route showed that the

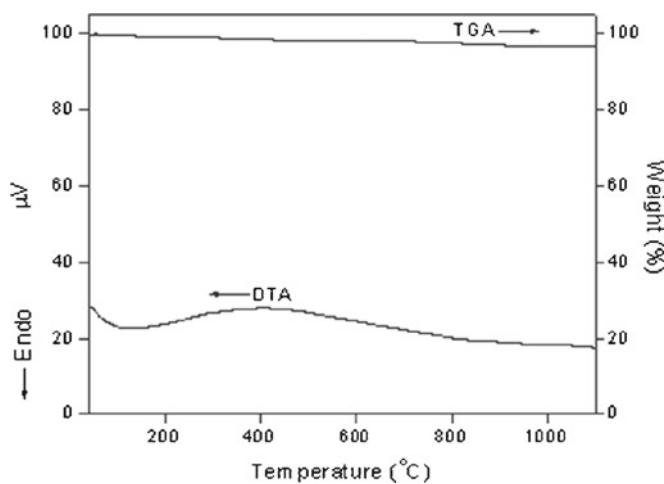


Figure 3. DTA/TGA curves of as-prepared $\text{NdBa}_2\text{ZrO}_{5.5}$ nanopowder.

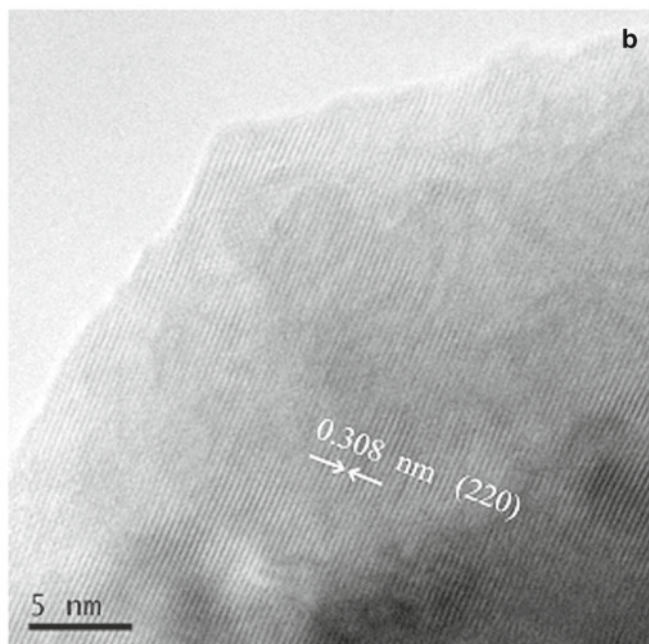
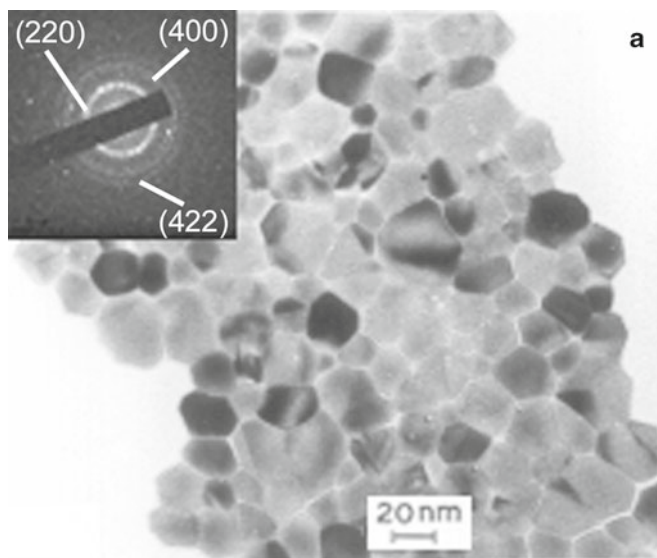


Figure 4. (a) TEM micrograph (inset shows corresponding SAED pattern) and (b) HRTEM lattice image of as-prepared $\text{NdBa}_2\text{ZrO}_{5.5}$ nanopowder.

Table 1. Lattice spacing for different crystal planes as measured from XRD and electron diffraction (ED) patterns of $\text{Ba}_2\text{NdZrO}_{5.5}$.

hkl	$d_{\text{XRD}} (\text{\AA})$	$d_{\text{ED}} (\text{\AA})$
220	3.028	3.080
400	2.119	2.116
422	1.729	1.722

particles are of submicron size in the range 20–30 nm as shown in figure 4a and the inset shows the corresponding selected area electron diffraction (SAED) pattern. The ring

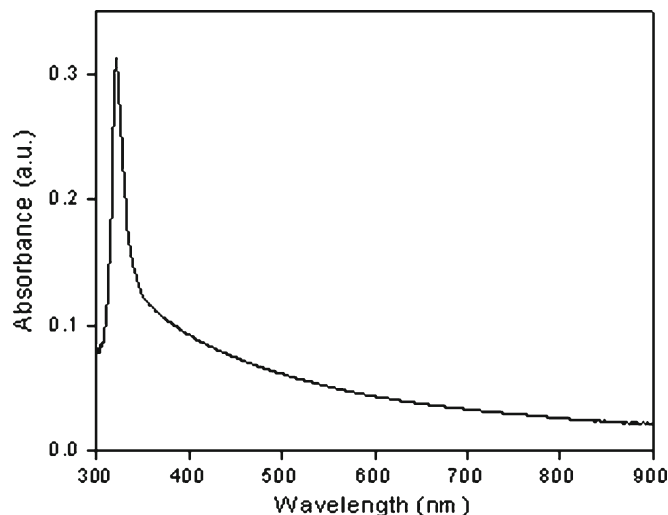


Figure 5. UV-absorption spectrum of nanocrystalline $\text{NdBa}_2\text{ZrO}_{5.5}$.

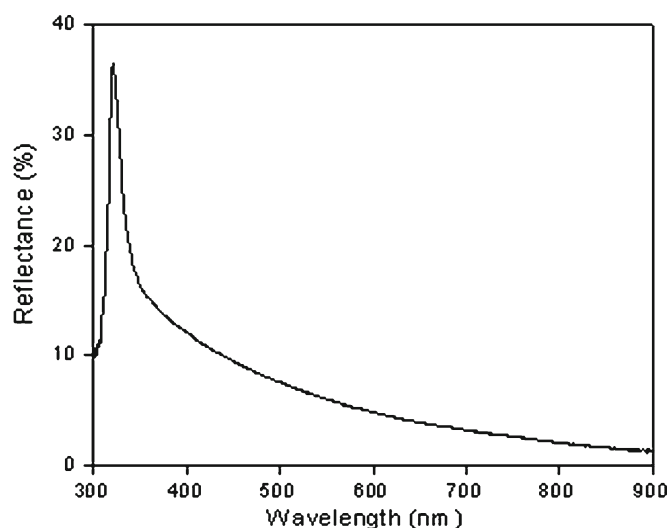


Figure 6. Variation of reflectance with wavelength for $\text{NdBa}_2\text{ZrO}_{5.5}$ nanopowder.

nature of the electron diffraction pattern is indicative of the polycrystalline nature of the crystallites, but the spotty nature of SAED can be due to the fact that the fine crystallites having related orientations are agglomerated together resulting in a limited set of orientations. The SAED pattern is indexed for a complex cubic perovskite structure and is in good agreement with the XRD data. Table 1 compares the lattice spacing (d) calculated from XRD and SAED patterns. Figure 4b is the high resolution lattice image (HRTEM) of the agglomerate sample which gives the crystal lattice stripe of the $\text{Ba}_2\text{NdZrO}_{5.5}$ particle. Indexing the lattice stripes, the typical lattice spacing corresponds to the interplanar spacing (d) of the (220) crystal plane which is 0.308 nm.

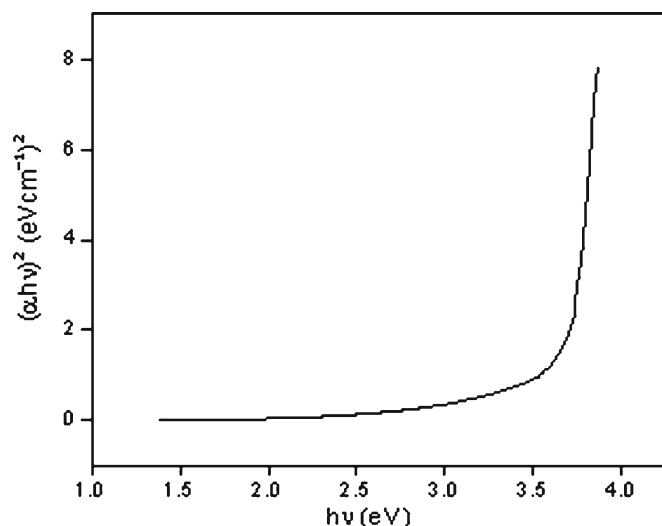


Figure 7. Energy bandgap determination of NdBa₂ZrO_{5.5} nanocrystals from $(\alpha hv)^2$ vs hv graph.

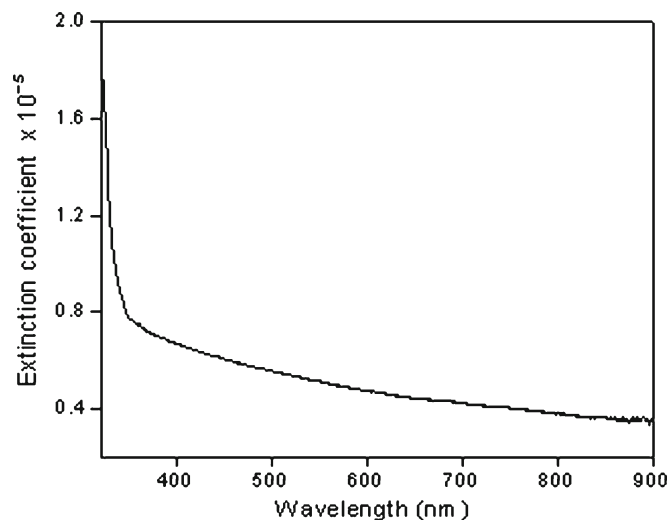


Figure 9. Variation of extinction coefficient with wavelength for nanocrystalline NdBa₂ZrO_{5.5}.

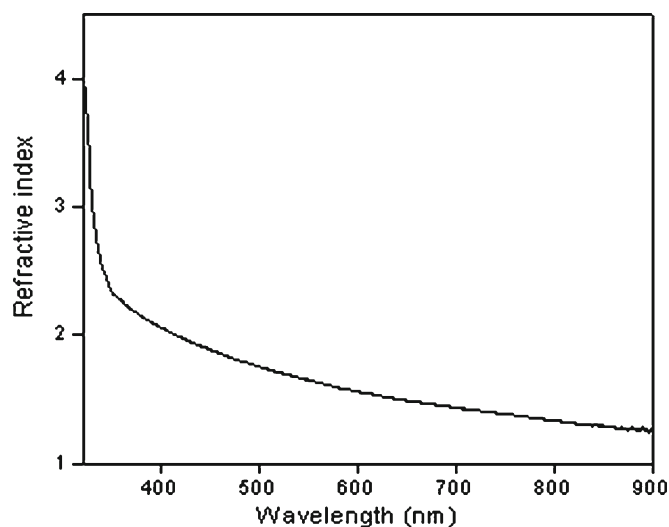


Figure 8. Variation of refractive index with wavelength for NdBa₂ZrO_{5.5} nanopowder.

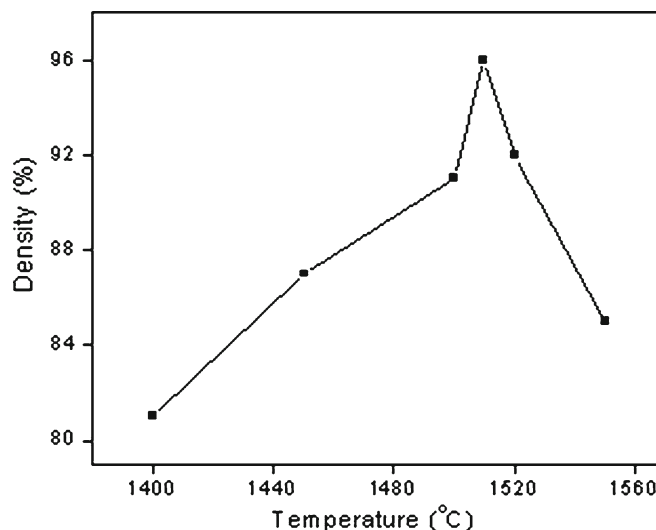


Figure 10. Variation of sintered density with temperature for NdBa₂ZrO_{5.5} pellet.

3.5 Optical absorption studies

The UV absorption and reflectance spectra of NdBa₂ZrO_{5.5} nanoparticles dispersed in hydrogen peroxide (at room temperature) are shown in figures 5 and 6, respectively. From the spectrograph the absorption edge was found to occur at ~336 nm. The existence of sharp absorption edge is the characteristics of crystalline state of the material which corroborates the XRD analysis. It is observed from the figures that absorbance and reflectance show peaks in the ultra-violet region and decreases sharply with increasing wavelength and becomes almost constant towards the visible region. The property of very low absorbance and reflectance in the visible region makes the material a good candidate as transparent windows in solar cells.

According to Tauc relation, the absorption coefficient for direct band material is given by (Tauc 1974; Sharma *et al* 1992)

$$\alpha hv = B (hv - E_g)^{1/2},$$

where B is a constant, α the absorption coefficient, hv the photon energy and E_g the bandgap. A graph between $(\alpha hv)^2$ vs hv is plotted and shown in figure 7. The extrapolation of straight line to $(\alpha hv)^2 = 0$ axis gives value of the energy bandgap of the material which is found to be ~3.69 eV. Since the bandgap of NdBa₂ZrO_{5.5} lies in the UV region, the material finds applications in the field of heterogeneous photocatalysis for the aqueous photodecomposition of organic contaminants. Recently, we have reported the photocatalytic

activities of complex perovskites under UV and solar light irradiations (Kumar *et al* 2011).

The variation of refractive index (n) and extinction coefficient (k) with wavelength of incident photon is shown in figures 8 and 9, respectively. Both n and k decrease exponentially with wavelength. The variations of n and k values in the investigated frequency range show that some interactions take place between photons and electrons. It is found that n and k show peaks around 4.0444 and 1.8217×10^{-5} which is at the same photon energy, 3.8697 eV. Thus, at room temperature, nanocrystalline $\text{NdBa}_2\text{ZrO}_{5.5}$ falls to the semiconducting range with a bandgap of ~ 3.69 eV since the maximum value of refractive index (n) occurred at energy ranges near where the maximum change in k occurred (Greenway and Harbeke 1969). Therefore, the material could be used as transparent wide bandgap semiconductor.

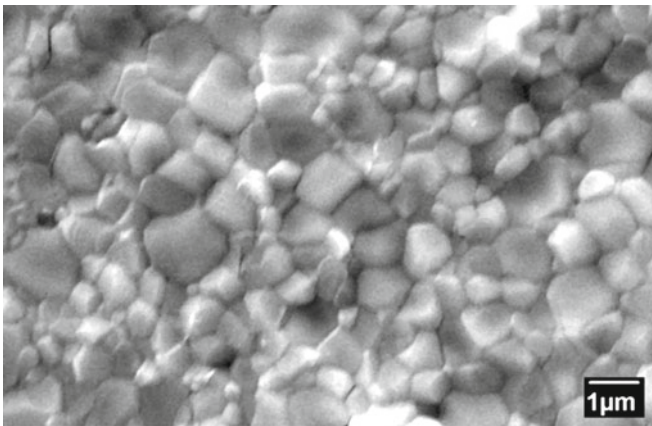


Figure 11. SEM secondary electron image of sintered pellet of $\text{NdBa}_2\text{ZrO}_{5.5}$.

3.6 Sintering and dielectric studies

The sintering behaviour of nanocrystals of $\text{NdBa}_2\text{ZrO}_{5.5}$ synthesized through the present combustion route was studied. The relative green density of the specimen used for the sintering study was $55 \pm 2\%$ for a pressure of 350 MPa. Figure 10 indicates a strong correlation between bulk density of the pellet and sintering temperature for a soaking time of 2 h. A sintered density of $\sim 96\%$ of the theoretical value was obtained on sintering the compacted specimen at 1510°C which seems to be very close to the optimum sintering temperature. Figure 11 shows SEM images of sintered specimen. No cracks or pores were observed on the surface. It is clear from the micrograph that densification was achieved without significant microstructural coarsening. The average grain size determined from SEM micrograph is ~ 700 nm.

The dielectric characteristics of $\text{NdBa}_2\text{ZrO}_{5.5}$ as a function of frequency measured at room temperature are shown in figure 12. Dielectric properties such as dielectric constant (ϵ_r) and loss factor ($\tan \delta$) of the polycrystalline $\text{NdBa}_2\text{ZrO}_{5.5}$ was studied in the frequency range 1 kHz to 5 MHz at room temperature. The value of ϵ_r is high at low frequencies and decreases rapidly as frequency increases. This is due to the fact that at lower frequencies, dipoles are able to follow the frequency of applied field; as frequency increases dipoles are not able to follow the frequency of applied field. The dielectric relaxation results in high value of dielectric constant at low frequencies and low value of dielectric constant at higher frequencies. The behaviour of decrease of $\tan \delta$ with increase in frequency is consistent with that of the dielectric constant of the sample. The specimen showed a moderate dielectric constant ($\epsilon_r = 29.6$) and loss factor ($\tan \delta = 4 \times 10^{-2}$) at 5 MHz frequencies at room temperature, which indicates that the material is suitable for microwave applications.

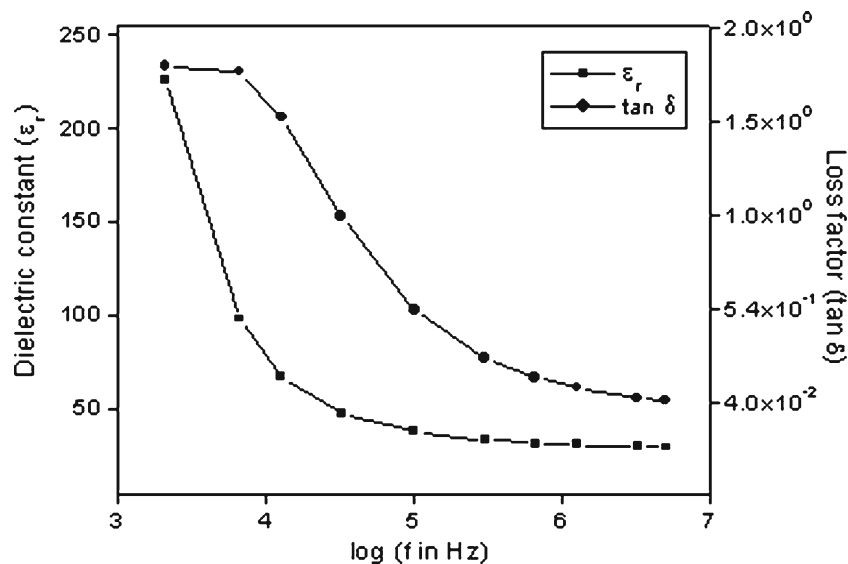


Figure 12. Variation of dielectric constant (ϵ_r) and loss factor ($\tan \delta$) with frequency.

4. Conclusions

The single step auto-ignition combustion technique was employed to synthesize nanocrystalline NdBa₂ZrO_{5.5}. X-ray diffraction studies have shown that the combustion product is phase pure NdBa₂ZrO_{5.5} and has a complex cubic perovskite structure. There was no evidence for the presence of any organic matter in the sample as suggested by FT-IR analysis. TG/DTA studies revealed that no phase transition occurs in the as-prepared powder at high temperatures. TEM micrographs confirmed the nanoscale size (20–30 nm) of the particles. SAED image shows that the oxide material is polycrystalline in nature. The lattice planes in HRTEM image indicate that even the smallest particles are reasonably well crystallized. The UV-VIS spectrum analysis revealed that the material is a wide bandgap ($E_g = 3.69$ eV) semiconductor at room temperature. The nanocrystals of NdBa₂ZrO_{5.5} could be sintered to ~96 % of the theoretical density at a temperature of 1510 °C for 2 h. SEM image of the sintered specimen indicates high densification of the material with an average grain size of ~700 nm. The room temperature dielectric constant (ϵ_r) and loss factor ($\tan \delta$) of the sintered specimen indicates that the material is suitable for microwave applications.

References

- Blasse G and Corsmit A F 1973 *J. Solid State Chem.* **6** 513
- Corsmit A F, Hoefdraad H F and Blasse G 1972 *J. Inorg. Nucl. Chem.* **34** 3401
- Glieter H 2000 *Acta Mater.* **48** 1
- Goodenough J B 1971 *Prog. Solid State Chem.* **5** 145
- Greenway D L and Harbeke G 1969 *Optical properties and band structures of semiconductors* (New York: Pergamon)
- Karagedov G R and Lyakhov N Z 1999 *Nanostruct. Mater.* **11** 559
- Kimura T and Tokura Y 2000 *Ann. Rev. Mater. Sci.* **30** 451
- Kumar V R, Prasad V S, Wariar P R S and Koshy J 2011 *NANO: Brief Reports and Reviews* **6** 279
- Lavat A E, Grasselli M C, Baran E J and Mercader R C 2001 *Mater. Lett.* **47** 194
- Lichtenburg F, Herrnberger A, Weidenmann K and Mannhart J 2001 *Prog. Solid State Chem.* **29** 1
- Nakamoto K 1986 *Infrared and Raman spectra of inorganic and coordination compounds* (New York: Wiley) 4th ed.
- Nyquist R N and Kagel R O 1971 *Infrared spectra of inorganic compounds* (New York: Academic Press)
- Osterloh F E 2008 *Chem. Mater.* **20** 35
- Ratheesh R, Sreemoolanadhan H and Sebastian M T 1997 *J. Solid State Chem.* **131** 2
- Ravichandran D, Roy R, Ravindranathan P and White W 2004 *J. Am. Ceram. Soc.* **82** 1082
- Sharma T P, Sharma S K and Singh V 1992 *CSIO Commun.* **19** 63
- Skandan G, Chen Y J, Glumac N and Kear B H 1999 *Nanostruct. Mater.* **11** 149
- Suryanarayana C 1994 *Bull. Mater. Sci.* **17** 307
- Tauc J (ed.) 1974 *Amorphous and liquid semiconductors* (New York: Plenum) p. 159
- Tovar H, Ortiz Díaz O, Landínez Téllez D A and Roa-Rojas J 2007 *Phys. Status Solidi (c)* **4** 4294
- Zheng W, Pang W and Meng G 1998 *Mater. Lett.* **37** 276